| | |
|---|---|
| AUTHOR | Jarkko Niemelä, Mari Partanen, Jarkko Ojala, Mika Kapanen and Jani Keyriläinen |
| TITLE | Dose-area product ratio in external small-beam radiotherapy: beam shape, size and energy dependencies in clinical photon beams |
| YEAR | 2021 |
| DOI | 10.1088/2057-1976/abf6aa |
| VERSION | Author's Accepted Manuscript |
| CITATION | Jarkko Niemelä et al 2021 Biomed. Phys. Eng. Express 7 035019 |

Title-page

# Dose-area product ratio in external small-beam radiotherapy: beam shape, size and energy dependencies in clinical photon beams

**Niemelä Jarkko[1,2,3], Partanen Mari[4,5], Ojala Jarkko[4,5], Kapanen Mika[4,5], Keyriläinen Jani[2,3]**
[1]University of Turku, Department of Physics and Astronomy, FI-20014 Turku, Finland
[2]Department of Medical Physics, Turku University Hospital, P.O.Box 52, FI-20521 Turku, Finland
[3]Department of Oncology and Radiotherapy, Turku University Hospital, P.O.Box 52, FI-20521 Turku, Finland
[4]Department of Oncology, Unit of Radiotherapy, Tampere University Hospital, P.O. Box 2000, FI-33521 Tampere, Finland
[5]Department of Medical Physics, Medical Imaging Center, Tampere University Hospital, P.O. Box 2000, FI-33521 Tampere, Finland

## Abstract

In small-field radiotherapy (RT), a significant challenge is to define the amount of radiation dose absorbed in the patient where the quality of the beam has to be measured with high accuracy. The properties of a proposed new beam quality specifier, namely the dose-area-product ratio at 20 and 10 cm depths in water or $DAPR_{20,10}$, were studied to yield more information on its feasibility over the conventional quality specifier tissue-phantom ratio or $TPR_{20,10}$. The $DAPR_{20,10}$ may be measured with a large-area ionization chamber (LAC) instead of small volume chambers or semi-conductors where detector, beam and water phantom positioning and beam perturbations introduce uncertainties. The effects of beam shape, size and energy on the $DAPR_{20,10}$ were studied and it was shown that the $DAPR_{20,10}$ increases with increasing beam energy similarly to $TPR_{20,10}$ but in contrast exhibits a small beam size and shape dependence. The beam profile outside the beam limiting devices has been shown to have a large contribution to the $DAPR_{20,10}$. There is potential in large area chambers to be used in DAPR measurement and its use in dosimetry of small-beam RT for beam quality measurements.

**Keywords**: small-beam dosimetry, stereotactic radiation therapy, dose-area product, beam quality parameter, EGSnrc, Monte Carlo

# Dose-area product ratio in external small-beam radiotherapy: field shape, size and energy dependencies in clinical photon beams

## Introduction

In radiotherapy (RT), small-field dosimetry is more challenging than conventional large field dosimetry established by IAEA TRS-398 and AAPM TG-51 dosimetry protocols. In 2017, IAEA and AAPM published a code of practice (CoP) TRS-483 for reference and relative dose determination in small static fields (IAEA TRS-483). This CoP describes the small-field dosimetry specific issues including the loss of lateral charged particle equilibrium and partial radiation source occlusion, detector and beam placement uncertainty as well as volume averaging of detector signal. These were also studied in several earlier publications (Li *et al*. 1995, Das *et al*. 2008, Alfonso *et al*. 2008, Charles *et al*. 2014, Benmakhlouf *et al*. 2014). The uncertainties from detector and beam placement and volume averaging in beam quality, output factor (OF) or absolute point dose determination in small beams could be overcome by the dose-area product (DAP) measurement with a large-area ionization chamber (LAC). With LACs, OFs have been determined through DAP measurements (Djouguela *et al*. 2006, Sánchez-Doblado *et al*. 2007) and the feasibility of DAP ratio (DAPR) has been studied as a beam quality specifier (Niemelä *et al*. 2017, Pimpinella *et al*. 2018). The use of DAP in absolute dosimetry and the establishment of a calibration coefficient for DAP in water, or $DAP_w$, has been studied (Dufreneix *et al*. 2016a, 2016b, Kupfer *et al*. 2017). In this work, the effects of beam shape, size and energy on the DAP ratio at 20 and 10 cm depths in water ($DAPR_{20,10}$) has been studied to further determine the usability of the $DAPR_{20,10}$ as a beam quality specifier in small clinical photon RT beams.

## Methods

*Measurements*

$DAPR_{20,10}$ is the ratio of the DAP at 20 cm depth with source-to-surface-distance (SSD) of 80 cm and the DAP at 10 cm depth with SSD of 90 cm, similarly to the definition of $TPR_{20,10}$.

We have investigated the $DAPR_{20,10}$ index with two large-area ionization chambers (LAC), namely Bragg Peak chamber Type 34070 (PTW.70) and Type 34073 (PTW.73) manufactured by PTW-Freiburg (PTW-Freiburg GmbH, Freiburg, Germany). Both LACs have an air volume thickness of 2.0 mm. The outer diameter of the PTW.70 is 104.0 mm and has an entrance window corresponding to 4.0 mm water-equivalent thickness for 6 MV photon beam. The diameters of the air volume and the active volume are 84.0 mm and 81.6 mm, respectively. The outer diameter of the PTW.73 is 68.0 mm and has an entrance window corresponding to 1.29 mm water-equivalent thickness for 6 MV beam. The diameters of the air volume and the active volume are 48.0 mm and 39.6 mm, respectively. The inner surface of the entrance window was used as the effective point of measurement for both LACs. The measured charge values were corrected for ambient conditions.

Measurements were carried out at Tampere University Hospital (Tays, Tampere, Finland) and Turku University Hospital (Tyks, Turku, Finland) using various beam types including conical collimators (CC) (Brainlab AG, Munich, Germany) from 4 to 15 mm in diameter, square jaw-defined beams from 10 to 200 mm in size and square MLC-shaped beams from 5 to 20 mm in size with three different medical linear accelerators (linacs) including Varian Clinac iX and two Varian TrueBeam (Varian Medical Systems, Inc., Palo Alto, CA, USA) linacs. Studied beam energies included conventional flattening filter (FF) beams with nominal energies of 6 and 18 MV and flattening filter-free (FFF) beams with nominal energies of 6 and 10 MV.

*$DAPR_{20,10}$ with beam shape and intensity*

The effect of field shape and intensity distribution to $DAPR_{20,10}$ were studied. Six field versions of varying shapes and intensities but equal size of 10 x 10 $mm^2$ delineated by MLCs were measured, as presented in figure 1. Linac jaws were chosen to form a 20 x 20 $mm^2$ opening centered at isocenter for versions 1 (v. 1) to 5 (v. 5) and offset laterally by 15 mm from isocenter for version 6 (v. 6). The center of a LAC was always positioned in the beam central axis (CAX). Measurements were performed for 6 MV FFF beam with PTW.73 and PTW.70 LACs. It is obvious that by moving an MLC aperture from the isocenter in FFF beams will produce a decreased intensity relative to the CAX, as compared with FF beams where the intensity is relatively constant due to flattened beam profile.

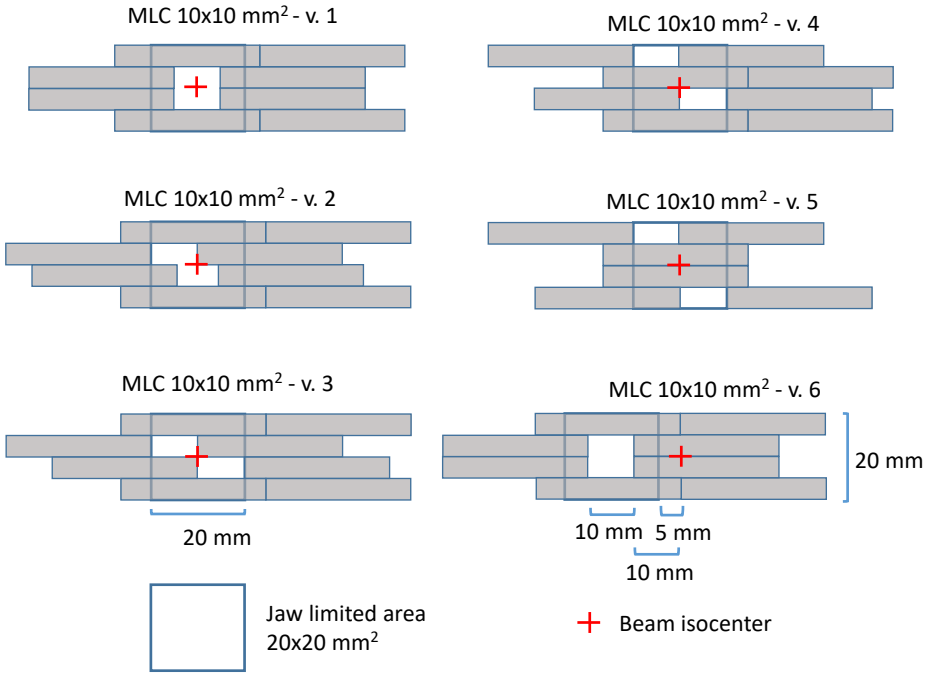


**Figure 1.** Diagrams of six different MLC-shaped fields, where the width of a leaf is 5 mm.

*Monte Carlo calculations*

Monte Carlo (MC) calculations were performed with the EGSnrc (v2017) code package (Kawrakow *et al*. 2016). The geometry model of the Varian Clinac iX has been modelled with the BEAMnrc user code included in the EGSnrc (Ojala *et al*. 2010, Ojala *et al*. 2014a, Ojala *et al*. 2014b and Ojala *et al*. 2014c). The MC model of Varian TrueBeam was based on phase-space (phsp) files provided by the manufacturer scored at the level before the jaws, which were used as a source in subsequent BEAMnrc treatment head simulation. The input file for the rest of the treatment head by the authors contained the jaws, an approximation of the collimator baseplate, the MLC in a park position, the light field reticle, and the interface mount with the geometrical and material details provided by the manufacturer. The CCs of size from 4 mm to 15 mm were modelled as per manufacturer specifications. The phsp files generated by the linac beam models were used as particle sources in the dose calculations in phantom with the egs_chamber user code. In all EGSnrc simulations, the transport parameters were ECUT = 0.521 MeV; PCUT = 0.001 MeV; Global SMAX = $1 \times 10^{10}$; ESTEPE = 0.25; XImax = 0.5; skin depth for BCA = 3; boundary crossing algorithm = EXACT; electron-step algorithm = PRESTA-II; spin effects = on; Brems angular sampling = KM; Brems cross sections = NIST; photon cross sections = xcom; electron impact ionization = On; triplet production = On; radiative Compton corrections = On; bound Compton scattering = On; pair angular sampling = KM; pair cross sections = NRC; photoelectron angular sampling = On;

Rayleigh scattering = On; atomic relaxations = On; photonuclear attenuation = On. In addition, for improving the simulation efficiency the photon cross-section enhancement was turned on with an enhancement factor of 128 with egs_chamber.

The MC calculations of $DAPR_{20,10}$ were performed in the water volume, the air volume and the active air volume of the two LACs, and are described in detail in earlier work (Niemelä *et al*. 2017). In the MC calculations, the water volumes were centered at the depth of 10 or 20 cm, while the upper surface of the air volumes and the LAC air volumes were set to 10 or 20 cm depth in the water phantom. The dose was scored in the active air volumes of the LACs, namely with diameters of 39.6 mm and 81.6 mm for the PTW.73 and PTW.70 chambers, respectively. The doses scored at the depths of 10 and 20 cm, with SSDs of 90 and 80 cm, respectively, were applied to calculate the DAPRs. The authors received confidential detailed geometrical and material information from the manufacturer PTW-Freiburg. This information was used for the detector construction in the egs_chamber simulations.

Moreover, 6 MV simulated parallel beams with diameters of 0.2 mm, 7.5 mm and 15 mm were studied to compare the $DAPR_{20,10}$ values to corresponding measured beam limiting device generated beams, such as CCs and MLCs. For simulated parallel beams, a spectrum from a small jaw-collimated (10 x 10 $mm^2$) FF beam of Varian TrueBeam linac was used. The phsp file was scored after the jaws at 45 cm distance from target level and the photon energy spectrum was determined using BEAMDP software included in EGSnc, inside an area of 7 x 7 $mm^2$ to form the parallel beam energy spectrum, as shown in figure 2. This area covers the complete jaw opening with a margin of 1.25 mm at all sides. The scored spectrum represents a close approximation of realistic small-field spectra with linacs used in this study. A similar energy spectrum has been scored in other papers (W. Ulmer 2013, Brualla *et al*. 2019) under the flattening filter. It can be seen from figure 2 that photon energy fluence through the jaws is from 3 to 5% of the photon energy fluence not through the jaws for the energies between/from 0.5 MeV and/to 5 MeV, respectively. The electron kinetic energy fluence is less than 0.1% of the in-field energy fluence. Simulated parallel beams starting at a plane located at 45 cm distance from the source are transported through a slab of air of 35 cm and 45 cm thick for SSD of 80 cm and 90 cm, respectively, before impinging on the water phantom. The doses to the water volumes, the air volumes and the active air volumes of detailed LAC were calculated, as described above. In addition, the $DAPR_{20,10}$ values for a 7.5 mm CC beam from our earlier work (Niemelä *et al*. 2017) were calculated as a function of the radius of the dose integral (integrated dose radius) ratios, or $DAP_{20}$ to $DAP_{10}$ ratio, in water and compared with the parallel beams. Integrated dose radius is the radius of the integrated dose to calculate the DAP values as a function of the scored slab radius. When calculated at both 10 and 20 cm depths, the $DAPR_{20,10}$ may be calculated.

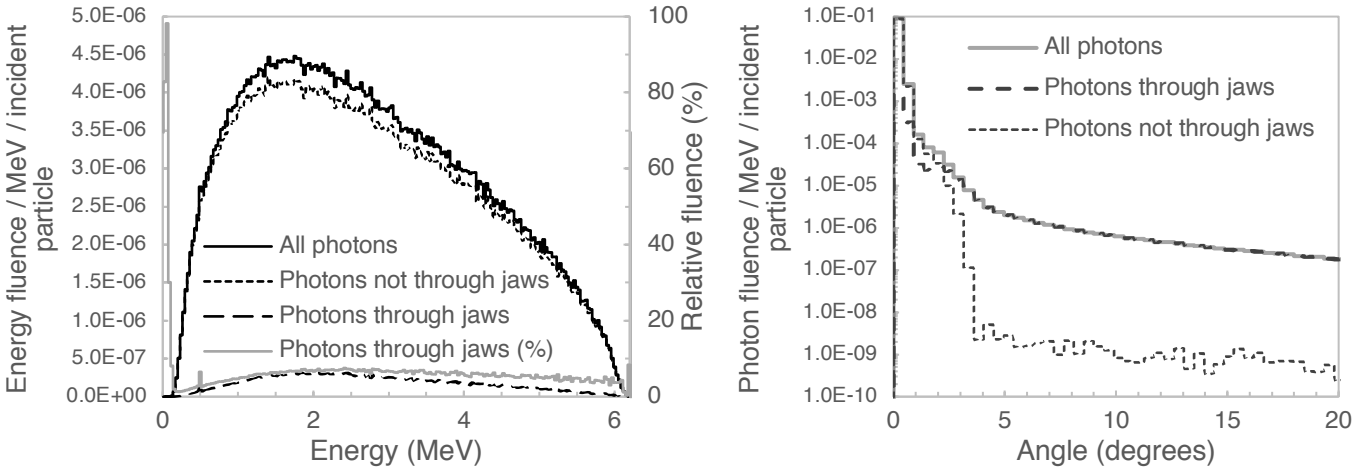


**Figure 2.** Scored energy spectra fluences (left) and an angular distribution of photon fluence (right) inside of 7 x 7 $mm^2$ area of a 10 x 10 $mm^2$ field (defined at 100 cm distance from the target) just after the jaws at 45 cm distance from the target.

**Results**

The $DAPR_{20,10}$ indexes measured with two LACs for three linacs, four beam energy types and various field sizes and shapes are presented in table 1. For clarity and a holistic view, earlier measured $DAPR_{20,10}$ values for 6 MV FF beams with CCs from 4 to 40 mm in diameter are presented (Niemelä *et al*. 2017). Later in the Discussion section parts of these tables are re-tabulated for further analysis.

**Table 1.** Measured dose-area-product ratio ($DAPR_{20,10}$) indexes for PTW34073 and PTW34070 LACs (LAC = large-area ionization chamber, linac = linear accelerator, FS = jaw-defined field size, Cone = diameter of conical collimator, MLC = multi-leaf collimator, FF = flattening filter, FFF = flattening filter-free, TB = TrueBeam).

| | | | | PTW34073 | | | | PTW34070 | | | |
|---|---|---|---|---|---|---|---|---|---|---|---|
| | | | | Beam type (nominal energy and flattening filter) | | | | | | | |
| Linac | FS (mm) | Cone (mm) | MLC (mm) | 6 MV FF | 18 MV FF | 6 MV FFF | 10 MV FFF | 6 MV FF | 18 MV FF | 6 MV FFF | 10 MV FFF |
| Clinic2 iX | 50 | 4 | - | 0.656* | 0.751 | - | - | 0.702* | 0.777 | - | - |
| Clinic2 iX | 50 | 7.5 | - | 0.635* | 0.746 | - | - | 0.674* | 0.774 | - | - |
| Clinic2 iX | 50 | 10 | - | 0.632* | 0.745 | - | - | 0.663* | 0.769 | - | - |
| Clinic2 iX | 50 | 20 | - | 0.626* | 0.745 | - | - | 0.655* | 0.770 | - | - |
| Clinic2 iX | 50 | 30 | - | 0.626* | 0.756 | - | - | 0.651* | 0.770 | - | - |
| Clinic2 iX | 50 | 40 | - | - | - | - | - | 0.651* | 0.770 | - | - |
| Clinic2 TB | 20 | 4 | - | - | - | 0.606 | 0.677 | - | - | - | - |
| Clinic2 TB | 20 | 7.5 | - | - | - | 0.596 | 0.674 | - | - | - | - |
| Clinic2 TB | 20 | 10 | - | - | - | 0.597 | 0.671 | - | - | - | - |
| Clinic2 TB | 20 | 15 | - | - | - | 0.593 | 0.673 | - | - | - | - |
| Clinic1 TB | 10 | - | - | - | - | - | - | - | - | 0.625 | 0.697 |
| Clinic1 TB | 20 | 4 | - | - | - | 0.603 | - | - | - | 0.635 | 0.705 |
| Clinic1 TB | 20 | 7.5 | - | - | - | 0.597 | - | - | - | 0.622 | 0.697 |
| Clinic1 TB | 20 | 10 | - | - | - | 0.596 | - | - | - | 0.620 | 0.696 |
| Clinic1 TB | 20 | 15 | - | - | - | 0.594 | - | - | - | 0.617 | 0.694 |
| Clinic1 TB | 20 | - | 5 | 0.640 | - | 0.619 | - | 0.663 | - | 0.644 | - |
| Clinic1 TB | 20 | - | 10 | 0.629 | - | 0.605 | - | 0.657 | - | 0.627 | - |
| Clinic1 TB | 20 | - | 15 | 0.625 | - | 0.598 | - | 0.652 | - | 0.622 | - |
| Clinic1 TB | 20 | - | 20 | 0.624 | - | 0.594 | - | 0.647 | - | 0.611 | - |
| Clinic1 TB | 20 | - | - | 0.626 | - | 0.593 | - | - | - | - | 0.688 |
| Clinic1 TB | 20 | - | 10v2 | - | - | 0.603 | - | - | - | 0.625 | - |
| Clinic1 TB | 20 | - | 10v3 | - | - | 0.600 | - | - | - | 0.626 | - |
| Clinic1 TB | 20 | - | 10v4 | - | - | 0.600 | - | - | - | 0.620 | - |
| Clinic1 TB | 20 | - | 10v5 | - | - | 0.601 | - | - | - | 0.620 | - |
| Clinic1 TB | 20 | - | 10v6 | - | - | 0.601 | - | - | - | 0.625 | - |
| Clinic1 TB | 30 | - | - | 0.629 | - | - | - | - | - | - | - |
| Clinic1 TB | 50 | 4 | - | - | - | 0.625 | - | - | - | 0.671 | 0.724 |
| Clinic1 TB | 50 | 7.5 | - | - | - | 0.605 | - | - | - | 0.638 | 0.707 |
| Clinic1 TB | 50 | 10 | - | - | - | 0.600 | - | - | - | 0.630 | 0.702 |
| Clinic1 TB | 50 | 15 | - | - | - | 0.596 | - | - | - | 0.622 | 0.698 |
| Clinic1 TB | 50 | - | - | 0.633 | - | 0.601 | - | - | - | 0.619 | 0.690 |
| Clinic1 TB | 100 | - | - | 0.658 | - | 0.625 | - | - | - | 0.628 | 0.701 |
| Clinic1 TB | 200 | - | - | - | - | - | - | - | - | 0.664 | 0.728 |

*Reported in the previous work (Niemelä *et al*. 2017). Reprinted with permission from the authors and the publisher.

MC-calculated $DAPR_{20,10}$ indexes for two LACs are presented in table 2. Results for 6 MV photon beams of Varian TrueBeam with CCs from 4 to 15 mm in diameter and MC-generated parallel beams calculated in air volume or detector active volume are presented. MC calculation relative difference to measurement is also tabulated there, where both results exist.

**Table 2**. MC-calculated dose-area-product ratio ($DAPR_{20,10}$) indexes for two LACs in various beam types and field sizes for 6 MV beam with doses scored in air cavity and detector active volume (LAC = large-area ionization chamber, linac = linear accelerator, Varian TB PB = parallel beam spectrum derived from a 10x10 $mm^2$ beam with flattening filter of Varian TrueBeam linac, FFF = flattening filter-free, PB = parallel beam, DB = divergent beam, FS = parallel beam field size (for PB), or jaw-defined field size (for DB), Cone = diameter of conical collimator, MC = Monte Carlo).

| | | | | | | MC | | Measurement | | Difference to measurement (%) | |
|---|---|---|---|---|---|---|---|---|---|---|---|
| Modeled linac | Flattening filter | Beam type | Volume | FS (mm) | Cone (mm) | PTW. 73 | PTW. 70 | PTW. 73 | PTW. 70 | PTW. 73 | PTW. 70 |
| Varian TB PB | - | PB | Air | 0.2 | - | 0.634 | 0.652 | - | - | - | - |
| Varian TB PB | - | PB | Detector | 0.2 | - | 0.633 | 0.652 | - | - | - | - |
| Varian TB PB | - | PB | Detector | 7.5 | - | 0.633 | 0.653 | - | - | - | - |
| Varian TB PB | - | PB | Detector | 15 | - | 0.634 | 0.652 | - | - | - | - |
| Clinic1 TB | FFF | DB | Detector | 20 | 4 | 0.604 | 0.625 | 0.603 | 0.635 | 0.2 | -1.5 |
| Clinic1 TB | FFF | DB | Detector | 20 | 7.5 | 0.597 | 0.615 | 0.597 | 0.622 | 0.0 | -1.1 |
| Clinic1 TB | FFF | DB | Detector | 20 | 15 | 0.595 | 0.613 | 0.594 | 0.617 | 0.3 | -0.7 |
| Clinic1 TB | FFF | DB | Detector | 50 | 4 | 0.622 | 0.656 | 0.625 | 0.671 | -0.5 | -2.2 |
| Clinic1 TB | FFF | DB | Detector | 50 | 15 | 0.596 | 0.616 | 0.596 | 0.622 | 0.0 | -0.9 |
| | | | | | | | | Average of differences: | | -0.0 | -1.3 |

To compare the variations of $DAPR_{20,10}$ with respect to beam size and shape, MC-calculated $DAPR_{20,10}$ values in water as a function of integrated dose radius for four different beams are shown in figure 3. These four beams are 0.2-mm-diameter parallel beam (PB0.2mm), 7.5-mm-diameter parallel beam (PB7.5mm), 15-mm-diameter parallel beam (PB15mm) and a fully simulated, cone collimated 7.5-mm-diameter beam with corresponding beam divergence (CC7.5mm) with jaw setting of 50 x 50 $mm^2$. Overall mean and maximum relative statistical uncertainties of the scored voxel doses to calculate $DAPR_{20,10}$ values in figure 3 were 0.1% and 0.9%, 0.1% and 3.2%, 0.1% and 3.9%, and 0.1% and 0.3%, respectively.

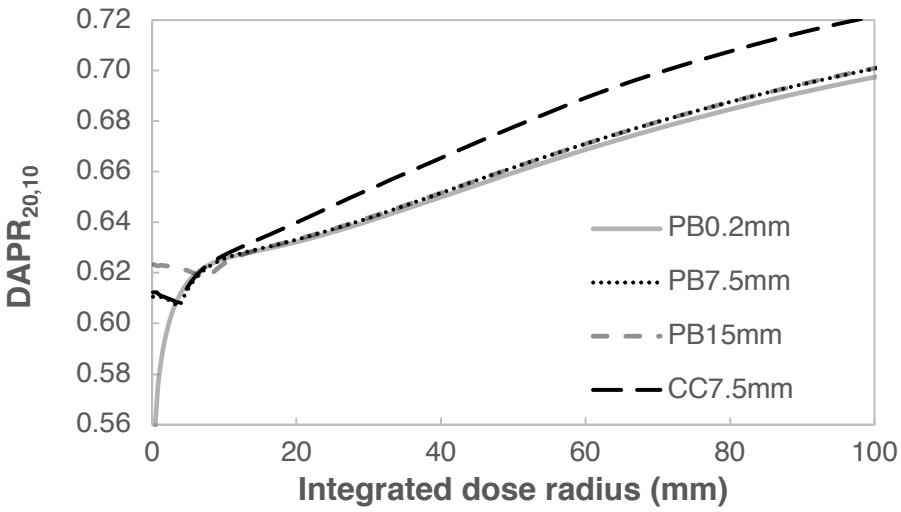


**Figure 3**. MC-calculated dose-area-product ratio ($DAPR_{20,10}$) values in water as a function of integrated dose radius for a parallel beam with diameter of 0.2 mm (PB0.2mm), 7.5 mm (PB7.5mm), 15 mm (PB15mm), a 7.5 mm diameter cone-collimated beam with flattening filter (CC7.5mm*) and jaw opening of 50 mm (MC = Monte Carlo, PB = parallel beam, CC = conical collimator).

*Result has been reported in the previous work (Niemelä *et al*. 2017). Reprinted with permission from the authors and the publisher.

**Discussion**

Studied $DAPR_{20,10}$ indexes are energy dependent similarly to the conventional $TPR_{20,10}$ indexes, namely the indexes increase with increasing energy as seen in table 1 for 6 , 10 and 18 MV energies. The field size dependence, however, is greatly reduced with the $DAPR_{20,10}$ compared with $TPR_{20,10}$ and earlier it has been reported that the $DAPR_{20,10}$ is field size independent (Dufreneix *et al*. 2016a, 2016b, Pimpinella *et al*. 2018). For FF beams and cones with diameters from 4 to 30 mm with jaw opening of 50 mm, the average $DAPR_{20,10}$ with one sigma standard deviation (SD) of 6 MV beam is 0.635 ± 0.011 and 0.669 ± 0.018 for PTW.73 and PTW.70 chambers, respectively, and SDs of 18 MV beam 0.749 ± 0.004 and 0.772 ± 0.003 for PTW.73 and PTW.70 chambers, respectively. The variation in $DAPR_{20,10}$ index is clearly smaller for the 18 MV FF beam with cone collimation compared with 6 MV beam for both chambers.

There is a moderate variation in $DAPR_{20,10}$ values with field shape and intensity as seen in table 3, which is re-tabulated from table 1 for clarity. The amount of change depends also on used LAC. The largest relative change of 1.2% was observed with larger LAC for the field shape versions of 4 and 5. The overall SDs of 0.3% and 0.5% for PTW.73 and PTW.70, respectively, suggest that the change in $DAPR_{20,10}$ is moderate when changes in field shape and intensity are present.

**Table 3.** Measured dose-area-product ratio ($DAPR_{20,10}$) indexes for PTW34073 and PTW34070 LACs with varying MLC field shapes and static 20 x 20 $cm^2$ jaw opening with Tyks Varian TB linear accelerator (LAC = large-area ionization chamber, MLC = multi-leaf collimator, Tyks = Turku University Hospital, TB = TrueBeam, SD = standard deviation).

| MLC | PTW.73 | Difference to v. 1 (%) | PTW.70 | Difference to v. 1 (%) |
|---|---|---|---|---|
| v. 1 | 0.605 | - | 0.627 | - |
| v. 2 | 0.603 | -0.4% | 0.625 | -0.4% |
| v. 3 | 0.600 | -0.8% | 0.626 | -0.2% |
| v. 4 | 0.600 | -0.9% | 0.620 | -1.2% |
| v. 5 | 0.601 | -0.6% | 0.620 | -1.2% |
| v. 6 | 0.601 | -0.7% | 0.623 | -0.7% |
| Mean | 0.602 | | 0.624 | |
| SD | 0.002 (0.3%) | | 0.003 (0.5%) | |

There is a substantial effect in the mechanism and geometry of the beam limiting devices affecting the $DAPR_{20,10}$ values. This can be noticed in figure 3 between the MC-calculated DAPR values for cone-collimated beam and the parallel beams, the cone collimation yielding larger DAPR values. In addition, it can be noted that the DAPR ratios approach the typical values of the $TPR_{20,10}$ of these beams when the integrated dose radius approaches 0 mm. This is actually the definition of the $TPR_{20,10}$, namely the dose in a point ratio at 20 and 10 cm depths. One can also observe the beam penumbras at 3.75 mm and 7.5 mm integrated dose radius for the 7.5 mm and 15 mm diameter beams.

In addition, it can be observed from table 4 (re-tabulated from table 1) that for an increase from 20 to 50 mm jaw opening, the $DAPR_{20,10}$ increases for constant cone diameter. This effect grows with smaller cone aperture diameters and thus, the $DAPR_{20,10}$ for the measured Clinic1 TB linac is 1.3% and 3.6% larger for 7.5-mm- and 4-mm-diameter cones, respectively. This can be explained by radiation penetration and scatter in the cones affecting the dose distribution outside of the cone-collimated field that the LAC chamber measures. The larger the jaw opening, the larger the contribution. The difference in $DAPR_{20,10}$ between the two Varian TB linacs at two different clinics is negligible.

**Table 4.** Measured dose-area-product ratio ($DAPR_{20,10}$) indexes with PTW.73 for cones and jaw-defined field sizes of 20 and 50 mm for 6 MV FFF beam (FFF = flattening filter-free, linac = linear accelerator, TB = TrueBeam).

| | | Diameter of conical collimator [mm] | | | |
|---|---|---|---|---|---|
| Jaws [mm] | Linac | 4 | 7.5 | 10 | 15 |

| | | | | | |
|---|---|---|---|---|---|
| 20 | Clinic2 TB | 0.606 | 0.596 | 0.597 | 0.593 |
| | Clinic1 TB | 0.603 | 0.597 | 0.596 | 0.594 |
| 50 | Clinic1 TB | 0.625 | 0.605 | 0.600 | 0.596 |

In table 5, the MC-calculated results for Varian iX linac published by Niemelä *et al*. (2017) and present results re-tabulated from table 2, show the similarity of $DAPR_{20,10}$ indexes between the parallel beams derived from an FF beam and cone collimated FF beams. For parallel beams of size from 0.2 to 15 mm in diameter, the $DAPR_{20,10}$ index is constant at 0.633 ± 0.001 and 0.652 ± 0.001 for PTW.73 and PTW.70 chambers, respectively. Clearly the size of the beam has very small effect on the index with constant beam energy. However, for the cones this is necessarily not the case if the size of upstream beam is much larger than the size of cone-defined beam (50 mm vs. 4 to 10 mm, respectively). In this beam geometry, there is a large contribution of dose to the DAP in the large periphery beyond the cone-limited beam, and the beam through the cones increases the $DAPR_{20,10}$ with 6 MV beam. This is further shown in the results for the largest cones of 20 and 30 mm in diameter, where the penetrated photon contribution to the DAP from a 50 mm jaw-defined beam is relatively smaller compared with the conical beams of 4-10 mm in diameter.

**Table 5**. MC-calculated dose-area-product ratio ($DAPR_{20,10}$) indexes for 6 MV FF cone beam (Varian iX) and parallel beam (Varian TB*) with field sizes from 0 to 30 mm for two LACs (FF = flattening filter, Varian TB* = parallel beam spectrum derived from a 1x1 $cm^2$ beam with flattening filter of Varian TrueBeam linear accelerator (linac), LAC = large-area ionization chamber, FS = parallel beam field size or jaw-defined field size for cones, Cone = diameter of conical collimator).

| Linac | FS (mm) | Cone (mm) | PTW.73 | PTW.70 |
|---|---|---|---|---|
| Varian iX | 50 | 4 | 0.658* | 0.693* |
| Varian iX | 50 | 7.5 | 0.641* | 0.667* |
| Varian iX | 50 | 10 | 0.639* | 0.661* |
| Varian iX | 50 | 20 | 0.633* | 0.654* |
| Varian iX | 50 | 30 | 0.633* | 0.652* |
| Varian TB* | 0.2 | - | 0.633 | 0.652 |
| Varian TB* | 7.5 | - | 0.633 | 0.653 |
| Varian TB* | 15 | - | 0.634 | 0.652 |

*Reported in the previous work (Niemelä *et al*. 2017).

It can be seen from table 2 that for parallel beam of 0.2 mm in diameter, the difference in $DAPR_{20,10}$ index is negligible for dose scored in complete LAC or air cavity in water. This has the implication that potential perturbation to the measured DAP is effectively cancelled out in DAPR value.

The LACs used in this study may exhibit a signal drift: 0.1% and 0.4% per hour has been demonstrated earlier for the PTW.70 and PTW.73 chambers, respectively (Pimpinella *et al*. 2018). If the measurements are carried out in less than an hour, the signal drift will have a small effect on the result. The drift should naturally be taken into account in absolute dose measurements.

In addition, there is a heterogenous response for these chambers (Kuess *et al*. 2017) resulting in response correction of up to 5%, and absolute dose measurements showed a 2.5 to 4.5% overestimation of the response for 6 x 6 $mm^2$ field size. However, as $DAPR_{20,10}$ is a ratio of signals at 10 and 20 cm depths, the heterogenous response should effectively cancel out.

A response curve has been determined for PTW.70 chamber (Fig. 6 in Kuess *et al*. 2017). After modifying the MC calculated dose profiles at 10 and 20 cm depths with the response curve, the resulting calculated $DAPR_{20,10}$ for CC7.5mm beam was 0.1% larger for chamber size of a PTW.70. This would be the value for the response correction factor. This implies that the response heterogeneity plays a role in the measurement of $DAPR_{20,10}$ in standards laboratory but is less significant in a clinic.

**Conclusion**

In this study, the properties of $DAPR_{20,10}$ was investigated with two large area plane parallel Bragg-peak ionization chambers (PTW.73 and PTW.70) for different small photon beam types including FF and FFF beams, CCs, MLC- and jaw-defined beams with nominal photon energies of 6, 10 and 18 MV. Comparisons were performed between measured and MC-calculated values of $DAPR_{20,10}$. The dependence of the $DAPR_{20,10}$ on beam setup and energy, and the minor dependence on field shape were demonstrated. The $DAPR_{20,10}$ increases with increasing beam energy similarly to $TPR_{20,10}$ but in contrast it exhibits only a small beam size and shape dependence. The beam profile outside of the beam limiting devices has been shown to contribute to the $DAPR_{20,10}$ with the implication that different beam limiting devices and geometries will produce varying $DAPR_{20,10}$ values that has to be taken into account, in particular in the absolute dosimetry. The respective beam profiles need to be determined accurately for used beam limiting devices and geometries.

The size of the reference area for the $DAPR_{20,10}$ index should be chosen in order to make the quality parameter feasible for the use in standard laboratories and transfer to clinics. This reference DAPR may be calculated with a simple correction factor, being simply a ratio of the DAPR values in the reference area and the measured area.

It can be concluded that there is a great potential with large area chambers to be used in dosimetry of small-beam RT for beam quality measurements to overcome the uncertainties in chamber, beam and

water phantom positioning as well as the small volume dosimeter-introduced perturbations in the $TPR_{20,10}$ measurement. With reduced uncertainties, also the measurement procedure could be faster.

**Acknowledgements**

This work was partially funded by the Finnish Cultural Foundation, Varsinais-Suomi Regional fund (grant 85151291). The authors wish to thank Mr. Pekka Aalto from Yanmedi Oy (Helsinki, Finland) and PTW-Freiburg GmbH (Freiburg, Germany) for a detector loan, and PTW-Freiburg for the delivery of confidential geometry and material composition information for the large-area ionization chambers PTW Type 30473 and PTW Type 30470.

**References**

AAPM American Association of Physicists in Medicine 1999 AAPM's TG-51 protocol for clinical reference dosimetry of high-energy photon and electron beams *Med. Phys.* **26** 1847-1870

Alfonso R *et al* 2008 A new formalism for reference dosimetry of small and nonstandard fields *Med. Phys.* **35** 5179–86

Benmakhlouf H, Sempau J and Andreo P 2014 Output correction factors for nine small field detectors in 6 MV radiation therapy photon beams: A PENELOPE Monte Carlo study *Med. Phys.* **41** (4) 041711

Brualla *et al*. 2019 PENELOPE/PRIMO-calculated photon and electron spectra from clinical accelerators *Rad. Onc.* **14** (6)

Charles P H, Cranmer-Sargison G, Thwaites D I, Crowe S B, Kairn T, Knight R T, Kenny J, Langton C M, and Trapp J V 2014 A practical and theoretical definition of very small field size for radiotherapy output factor measurements *Med. Phys.* **41** (4) 041707

Das I J, Ding G X and Ahnesjö A 2008 Small fields: nonequilibrium radiation dosimetry *Med. Phys.* **35** 206–15

Dufreneix S, Ostrowsky A, Le Roy M, Sommier L, Gouriou J, Delaunay F, Rapp B, Daures J and Bordy J-M 2016a Using a dose-area product for absolute measurements in small fields: a feasibility study *Phys. Med. Biol.* **61** 650–662

Dufreneix S, Ostrowsky A, Rapp B, Daures J and Bordy J-M 2016b Accuracy of a dose-area product compared to an absorbed dose to water at a point in a 2 cm diameter field *Med. Phys.* **43** 4085-4092

IAEA International Atomic Energy Agency 2000 Absorbed dose determination in external beam

radiotherapy: an international code of practice for dosimetry based on standards of absorbed dose to water Technical Report Series No. 398 IAEA, Vienna (www-pub.iaea.org/MTCD/publications/PDF/TRS398_scr.pdf)

IAEA International Atomic Energy Agency and AAPM American Association of Physicists in Medicine 2017 Dosimetry of Small Static Fields Used in External Beam Radiotherapy – An International Code of Practice for Reference and Relative Dose Determination Technical Reports Series No. 483

Kupfer T, Lehmann J, Butler DJ, Ramanathan G, Bailey TE, Franich RD 2017 Commissioning of a PTW 34070 large-area plane-parallel ionization chamber for small field megavoltage photon dosimetry *J. Appl. Clin. Med. Phys.* **18** (6) 206-207

Kuess P, Böhlen TT, Lechner W, Elia A, Georg D and Palmans H 2017 Lateral response heterogeneity of Bragg peak ionization chambers for narrow-beam photon and proton dosimetry *Phys. Med. Biol.* **62** 9189

Li X A, Soubra M, Szanto J and Gerig L H 1995 Lateral electron equilibrium and electron contamination in measurements of headscatter factors using miniphantoms and brass caps *Med. Phys.* **22** 1167–70

Niemelä J, Partanen M, Ojala J, Sipilä P, Björkqvist M, Kapanen M and Keyriläinen J 2017 Measurement and properties of the dose–area product ratio in external small-beam radiotherapy *Phys. Med. Biol.* **62** 4870–4883

Ojala J, Hyödynmaa S, Baranczyk R, et al. 2014 Performance of two commercial electron beam algorithms over regions close to the lung–mediastinum interface, against Monte Carlo simulation and point dosimetry in virtual and anthropomorphic phantoms. Phys. Med. **30** 147–154

Ojala J, Hyödynmaa S, Pitkänen M 2010 BEAMnrc Monte Carlo modelling of linear accelerator using parallel computing grid – validation of a common, fixed geometry model for photon and electron beams. Proceedings of XVIth ICCR, Amsterdam, The Netherlands.

Ojala JJ, Kapanen MK, Hyödynmaa SJ, et al. 2014 Performance of dose calculation algorithms from three generations in lung SBRT: comparison with full Monte Carlo-based dose distributions. J Appl Clin Med Phys. **15** 4662

Ojala J, Kapanen M, Sipilä P, Hyödynmaa S, Pitkänen M 2014 The accuracy of Acuros XB algorithm for radiation beams traversing a metallic hip implant – comparison with measurements and Monte Carlo calculations. J Appl Clin Med Phys. **15** 4912

Partanen M, Ojala J, Niemelä J, Björkqvist M, Keyriläinen J and Kapanen M 2017 Comparison of two Monte Carlo based codes for small-field dose calculations in external beam radiotherapy *Acta Oncol.* **56** 891-3

Pimpinella M, Caporali C, Guerra AS, Silvi L, De Coste V, Petrucci A, Delaunay F, Dufreneix X, Gouriou J, Ostrowsky A, Rapp 4B Bordy J-M, Daures J, Le Roy M, Sommier L, Vermesse D 2018

Feasibility of using a dose-area product ratio as beam quality specifier for photon beams with small field sizes *Phys Med*. **45** 106-116

Ulmer W 2013 Creation of High Energy/Intensity Bremsstrahlung by a Multi-Target and Focusing of the Scattered Electrons by Small-Angle Backscatter at a Cone Wall and a Magnetic Field—Enhancement of the Outcome of Linear Accelerators in Radiotherapy *Int. J. Med. Phys., Clin. Eng. Rad. Onc*. **2** 147-160